Studies of the phase gradient at the boundary of the phase diffusion equation, motivated by peculiar wave patterns of rhythmic contraction in the amoeboid movement of *Physarum polycephalum*

2017 J. Phys. D: Appl. Phys. 50 154004

(http://iopscience.iop.org/0022-3727/50/15/154004)

IOP Publishing Journal of Physics D: Applied Physics

J. Phys. D: Appl. Phys. **50** (2017) 154004 (10pp) https://doi.org/10.1088/1361-6463/aa6269

Studies of the phase gradient at the boundary of the phase diffusion equation, motivated by peculiar wave patterns of rhythmic contraction in the amoeboid movement of *Physarum polycephalum*

Makoto Iima[1], **Hiroshi Kori**[2] **and Toshiyuki Nakagaki**[3]

[1] Graduate school of Science, Hiroshima University, 1-7-1 Kagamiyama, Higashi-Hiroshima, Hiroshima, 739-0041, Japan
[2] Department of Information Sciences, Ochanomizu Univeristy, Tokyo 11 2-8610, Japan
[3] Research Institute for Electronic Science, Hokkaido University, N20 W10, Kita-ku, Sapporo, 001-0020, Japan

E-mail: makoto@mis.hiroshima-u.ac.jp

Received 30 November 2016, revised 24 January 2017
Accepted for publication 23 February 2017
Published 14 March 2017

Abstract

The boundary of a cell is the interface with its surroundings and plays a key role in controlling the cell movement adaptations to different environments. We propose a study of the boundary effects on the patterns and waves of the rhythmic contractions in plasmodia of *Physarum polycephalum*, a tractable model organism of the amoeboid type. Boundary effects are defined as the effects of both the boundary conditions and the boundary shape. The rhythmicity of contraction can be modulated by local stimulation of temperature, light and chemicals, and by local deformation of cell shape via mechanosensitive ion channels as well. First, we examined the effects of boundary cell shapes in the case of a special shape resembling a tadpole, while requiring that the natural frequency in the proximity of the boundary is slightly higher and uniform. The simulation model reproduced the approximate propagated wave, from the tail to the head, while the inward waves were observed only near the periphery of the head section of the tadpole-shape. A key finding was that the frequency of the rhythmic contractions depended on the local shape of cell boundary. This implies that the boundary conditions of the phase were not always homogeneous. To understand the dependency, we reduced the two-dimensional model into a one-dimensional continuum model with Neumann boundary conditions. Here, the boundary conditions reflect the frequency distribution at the boundary. We described the analytic solutions and calculated the relationship between the boundary conditions and the wave propagation for a one-dimensional model of the continuous oscillatory field and a discrete coupled oscillator system. The results obtained may not be limited to cell movement of *Physarum*, but may be applicable to the other physical systems since the analysis used a generic phase diffusion equation.

Keywords: boundary condition, coupled oscillator model, phase equation, *Physarum plasmodium*

(Some figures may appear in colour only in the online journal)

1. Introduction

The plasmodium is a giant amoeboid organism and the structure is composed of protoplasmic gel that contains protoplasmic sol inside. The size of the plasmodium ranges from hundreds micrometers to several meters. The protoplasmic sol shows periodic streaming due to periodic contraction/relaxation of the protoplasmic gel, which results in complex space-time patterns, such as a propagating wave and rotating wave of the flow and thickness. Various boundary shapes and the heterogeneity of the media lead to interesting wave properties; with refraction and diffraction being the most common properties. In the case of waves in an excitable media, boundary effects cause other important properties to be considered. Unidirectional wave propagation for a particular boundary shape [1], destruction of a wave front leading to the formation of a spiral wave by an obstacle [2], a spiral wave controlled by a global feedback in a domain [3], and front bifurcation of concentration waves [4] are a few examples that have been studied. However, the details of the spontaneous formation mechanism and the significance of such patterns have been an open question.

Coupled oscillator models are useful as a mathematical model of spontaneous formation of spatiotemporal patterns. We can regard a whole organism as an assembly of oscillators, each of which describes spontaneous oscillations of a small piece of the body. Such a model was recently used to study the relationship between the coupling strength and the sensing ability [5]. The oscillators have the possibility of having different natural frequencies and are coupled with one another by mechanical connections or chemical signals. Even a simple model shows various spatiotemporal patterns including a propagating wave, and the key mechanism underlying the formation of the wave is the synchronization of the oscillators [6]. Furthermore, by taking an appropriate continuum limit, one can reduce the coupled discrete oscillators to a partial differential equation, referred to as a phase diffusion equation, which is easier to analyze yet reproduces the various spatiotemporal patterns mentioned above [6]. Such a simple description is convenient to provide insight into the spatiotemporal patterns exhibited by slime molds.

Here we focus on the simple propagating waves of the body thickness observed in the following two situations. When the shape of the protoplasm is set to a rectangular shape on the order of a centimeter, a propagating wave is observed [7–9]. Also, in the case where the slime mold is put on an unbounded region and the body size is set to 100–300 μm, the body takes a tadpole-like shape, and a peculiar wave pattern is observed where it propagates from the tail (narrower region of body) to the head (wider region of body) and the phase velocity is significantly slower in the region near the end of the tail [10]. These experimental observations led us to consider the phase gradient at the end in relation to the boundary conditions. The non-zero gradient of a variable at the boundary has been known in the boundary condition of calcium wave as the flux across the plasma membrane into the cytoplasm [11]. Another example of the flux across a heterogeneous media can be seen in the wave propagation of the BZ reaction system [12]. In a simple system of linear wave equations, a numerical integration technique applicable for a wide range of boundary conditions—including the Neumann condition—is also discussed [13].

In these experiments, observed patterns are critically dependent on ambient conditions, that is, the surrounding environment and the shape of the considered region. In the first case, a favorite stimulus, such as a comfortable temperature for the organisms, is provided in a confined protoplasm, and the wave in the body propagates from an end included in the region. It is known that favorite stimulus such as food or comfortable temperature increases the oscillation frequency of the body part subjected to the stimulus. Such a region may serve as a wave source, as predicted by the phase diffusion equation [6]. In the second case, when a wave pattern is modeled by sectional oscillations, the wave pattern plays an important role in the net transport of passive scalar factors, corresponding to internal chemicals or nutrients [14]. In previously described models [14], the tadpole shape of slime mold is simplified to two regions oscillating independently. The phase of the oscillation is uniform in each region and the phase difference in the regions represents an inhomogeneous wave. Those experimental and theoretical studies suggest that the boundary effect is a key factor in determining the types of wave patterns observed in slime mold. However, most theoretical studies on pattern formation have employed restricted boundary conditions such as the Neumann boundary condition with zero gradient [15]. To understand peculiar patterns observed in slime mold, one needs to consider more general boundary conditions appropriate for each experimental setup.

We investigate the coupled discrete oscillators and its continuum limit in the following two setups, with special attention to the phase gradient at the boundary. The first system is a two dimensional system with a tadpole-like shape in which a uniform boundary state with a slightly higher frequency is applied in order to see how a specific shape of cell causes modulation of phase waves. In the second system, the two-dimensional system is reduced to a one-dimensional system in which different phase gradients are applied to the two ends of the system as the boundary conditions, resulting in models reproducing the peculiar wave pattern observed in the experiment.

Our results will be organized as follows. In section 2, experimental observation of a tadpole-shaped *Physarum* is briefly reviewed. In section 3, we will show that the coupled oscillator model with a tadpole shape causes a similar wave pattern to *Physarum* even if the natural frequency on the boundary is uniform. In section 4, we relate the natural frequency difference near the boundary to the boundary condition in the phase equation with a peculiar wave pattern observed in the slime mold with the tadpole shape, and the wave pattern giving us insight to the characteristics of the coupling function in the coupled oscillator description. In section 5, we briefly summarize the characteristics of both models.

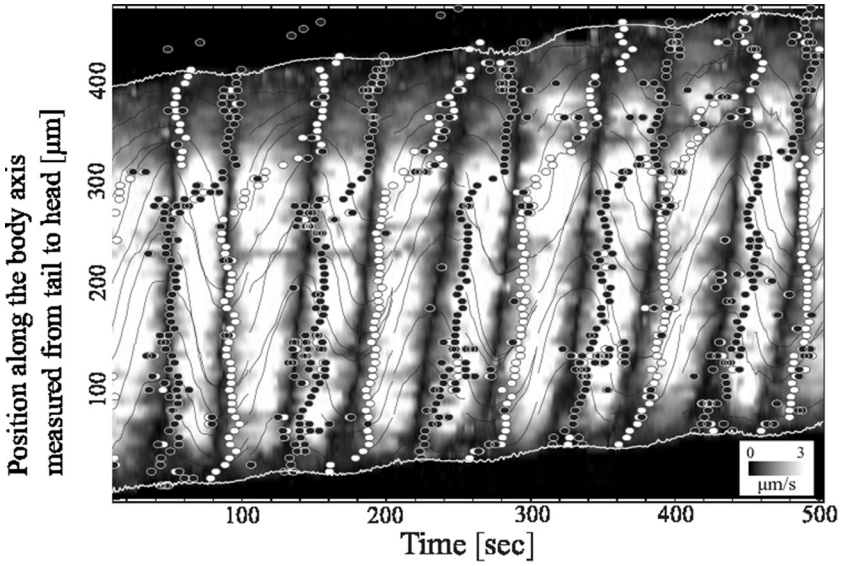

Figure 1. The spatiotemporal pattern of the tadpole-shaped slime mold (modified from [10], copyright 2008, with permission from Elsevier). Grayscale shows the flow speed and open circles and solid circles show the onset of contractions and relaxations, respectively.

2. Experimental phase patterns of the tadpole-shaped slime mold

In this section, we briefly review the observation of peristaltic motion of the tadpole-shaped *Physarum polycephalum* by Matsumoto *et al* [10] (see also [14]). The size is about 100–300 μm and the thickness is approximately 30 μm; thus the structure inside the body can be regarded as two-dimensional. It attaches to the base plate and moves from the tail to head. The thickness of the slime mold in the tail oscillates and the spatiotemporal pattern is a wave propagating from the tail to the head.

Figure 1 shows a spatiotemporal pattern of the thickness of the slime mold and the flow along a centerline of the tadpole shape [10, 14]. Isophase lines of the oscillation for the flow correspond to the dark region, and those for the thickness the open circles and black circles. Apparently, the gradient of the constant phase is relatively small near the tail, whereas the constant phase line fluctuates in the head part which can be roughly defined by $x > 300$ μm (for the detailed shape of the slime mold, see [10]). Such bending pattern of the constant phase is not observed when the phase wave has a spatially uniform phase velocity. Because each part of the slime mold oscillates with a natural frequency and they are coupled with each other via mechanical or chemical signals, a coupled oscillator model can be used to describe this pattern. In the following, we focus on the boundary condition at the tail end and consider the wave pattern of the phase equation under Neumann boundary condition.

3. Numerical simulation of a two-dimensional model

We hypothesize that the phase wave observed in a slime mold is propagated from a part subjected to a preferred stimulus, which increases the natural frequency of the stimulated part. In this section, we consider the effect of the boundary shape by considering a two-dimensional phase distribution in the tadpole region. We assume homogeneous boundary conditions with constant phase gradients, and focus on how the asymmetry of the shape in the anterior part and the posterior part causes the phase wave, in particular, the direction of the phase wave.

The tadpole-shape body and the boundary are denoted by B and ∂B, respectively. To implement the boundary of arbitrary shape, we first discretize a two-dimensional region $[0, L_x] \times [0, L_y]$ by rectangular meshes, $[i\Delta x, (i+1)\Delta x] \times [j\Delta y, (j+1)\Delta y]$ where $\Delta x = L_x/N_x$, $\Delta y = L_y/N_y$ and $0 \leqslant i < N_x$, $0 \leqslant j < N_y$. In the following, we assume that $\Delta x = \Delta y$ for simplicity. The mesh characterized by (i,j) is indicated by $\boldsymbol{x} = (i,j)$. We classify the meshes in the following three categories. The meshes occupied with the region B alone are indicated by B_i. The meshes including ∂B, defined by $\boldsymbol{x}$ such that $\boldsymbol{x} \notin B_{\mathrm{i}}$ and one of the conditions $(i \pm 1, j \pm 1) \in B_{\mathrm{i}}$ are satisfied, are indicated by B_b. Other meshes are regarded as the outside of the body. To describe them, we define a state function $s(\boldsymbol{x})$ as

$$s(\boldsymbol{x}) = \begin{cases} 0 & \boldsymbol{x} \in B_i, \\ 1 & \boldsymbol{x} \in B_b, \\ -1 & \text{otherwise.} \end{cases} \tag{1}$$

We used the coupling function $f(x) = -\sin(x + \Theta) + \sin\Theta$, where θ is a constant, and constructed the model by setting natural frequencies as follows; (1) the natural frequency of the oscillator in the region B_i is ω, a constant; (2) the natural frequency of the oscillator in the region B_b is $\omega + \Delta\omega$, another constant to represents the phase gradient of the boundary (the relationship between $\Delta\omega$ and the phase gradient of the boundary is discussed in section 4.1); (3) the coupling between sites in $B_i \cup B_b$ only is considered. The model used for the simulation was the following discretized phase equation for the phase $\phi(\boldsymbol{x}, t)$,

$$\frac{\mathrm{d}\phi(\boldsymbol{x},t)}{\mathrm{d}t} = \omega + s(\boldsymbol{x})\Delta\omega + \sum_{|\boldsymbol{x}-\boldsymbol{x}'|\leqslant 1} k(\boldsymbol{x},\boldsymbol{x}')f(\phi(\boldsymbol{x},t) - \phi(\boldsymbol{x}',t)), \quad (\boldsymbol{x} \in B_i \cup B_b) \tag{2}$$

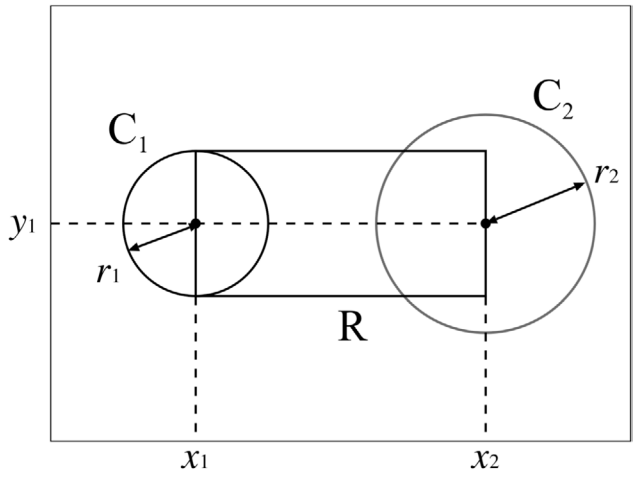

Figure 2. A tadpole region $B = C_1 \cup C_2 \cup R$, where C_1 and C_2 are circles of radii r_1 and r_2 centered at (x_1, y_1) and (x_2, y_1), and R is the rectangle of the size $(x_2 - x_1) \times 2r_1$. We define C_2 as the head, and $B \setminus C_2 = (C_1 \cup R) \cap \overline{C_2}$ as the tail.

and the phase dynamics in the region defined by $\boldsymbol{x} \notin B_i$ and $\boldsymbol{x} \notin B_b$ were omitted because they do not affect the dynamics of the phase in the region $B_i \cup B_b$. Here, $|\boldsymbol{x} - \boldsymbol{x}'|$ is the L^1 − norm (or the Manhattan distance) of the vector $\boldsymbol{x} - \boldsymbol{x}'$. The connectivity function $k(\boldsymbol{x}, \boldsymbol{x}')$ is:

$$k(\boldsymbol{x}, \boldsymbol{x}') = \begin{cases} k_0 & s(\boldsymbol{x}) \neq -1 \text{ and } s(\boldsymbol{x}') \neq -1 \\ 0 & \text{(otherwise)} \end{cases} \tag{3}$$

The region B is defined by two circles and one rectangular shown in figure 2.

We used the following parameters: $L_x = L_y = L = 2$, $\Theta = -0.7 \times \pi/2$, $k_0 = 0.005/\Delta x^2$, $\omega = 2\pi$, $\Delta\omega = 0.02 \times 2\pi/\Delta x$. Parameter $\Delta\omega$ should depend on Δx so that the product $\Delta\omega\Delta x$, which determines the phase gradient of the boundary, converges in the limit $\Delta x \to 0$. Similarly, parameter k_0 should proportional to Δx^{-2}. (For the continuous limit of the coupled oscillator model for the one dimensional case, see section 4.1). The tadpole shape is defined as $x_1 = 0.2L, x_2 = 0.75L, y_1 = L_y/2 = 0.5L, r_1 = 0.1L, r_2 = 0.2L$ and $\Delta t = 0.001$ and $N_x = N_y = N = 100$. The time evolution was calculated by the fourth-order Runge–Kutta method. We also performed numerical simulations using the same parameter values except $(N, \Delta t) = (150, 0.001), (100, 0.0005)$ as well as k_0 and $\Delta\omega$ to keep the products $k_0\Delta x^2$ and $\Delta\omega\Delta x$ constant, and confirmed that the following results do not depend on these parameters significantly.

The isophase lines in the region $B_i \cup B_b$ are shown in figure 3(top left). An asymmetric wave propagation from the tail to the head is shown. This asymmetry comes from the asymmetry of the shape of the tail and the head. In the case $r_1 = r_2$, the region $B_i \cup B_b$ is symmetric with respect to the line $x = (x_1 + x_2)/2$. The two-dimensional phase wave pattern is shown in figure 3(top right). Here, unidirectional wave propagation is not observed and the waves from the boundaries reach to the center of the region. In figure 3(bottom), spatio-temporal pattern of the phase corresponding to figure 3(top left), along the line $y = y_1$, is shown. This pattern in the tail part ($x < 0.55L$) is similar to the experimental results (figure 1).

In this model, the wave propagation was the result of the asymmetry of body shape in the head part and that in the tail part. The shape differences lead to the different details of inward waves from the boundary in each part. If the observed wave pattern were reduced to one-dimensional along the axis defined by $y = y_1$, this asymmetry causes a difference of the dominant region in the phase wave generated from the boundary. In the tadpole-shaped model, the wave pattern is dominated by the end of the tail region and the phase wave propagates to the center of the head region. Such a difference of the dominant regions can be achieved by the value of the phase gradient of the boundary, which is referred to in appendix. Furthermore, such differences can also be reproduced in the phase wave pattern similar to experimental observation in that the wave speed near the tail was slightly slower, yet it increased when the wave entered the head region. In the next section, we will consider a one dimensional model incorporating this wave property.

4. Boundary condition of the one-dimensional phase diffusion equation

4.1. Locally synchronized state and the boundary condition

In this section, we introduce a coupled oscillator model to investigate the relationship between the boundary condition of the phase diffusion equation and the inhomogeneity of the natural frequency at the end part.

We consider $N + 2$ coupled oscillators aligned on a line segment with equal distance, l. The equation of the system is given by

$$\frac{\mathrm{d}\phi_0}{\mathrm{d}t} = \omega_0 + \tilde{k} f(\phi_0 - \phi_1), \tag{4}$$

$$\frac{\mathrm{d}\phi_j}{\mathrm{d}t} = \omega_j + \tilde{k}\{f(\phi_j - \phi_{j-1}) + f(\phi_j - \phi_{j+1})\} \quad (j = 1, 2, \cdots, N), \tag{5}$$

$$\frac{\mathrm{d}\phi_{N+1}}{\mathrm{d}t} = \omega_{N+1} + \tilde{k} f(\phi_{N+1} - \phi_N), \tag{6}$$

where ϕ_j and ω_j $(j = 0, \cdots, N + 1)$ are the phases and the natural frequencies of the jth oscillator, respectively. $\tilde{k}(> 0)$ is a constant describing coupling strength, and $f(x)$ is a coupling function between adjacent oscillators. The coupling function $f(x)$ is periodic with the period 2π. Without loss of generality, we assume that $f(0) = 0$.

To consider the inhomogeneity at the both ends given by $j = 0, N + 1$, we assume that $\omega_0 = \omega + \Delta\omega_0, \omega_j = \omega$ $(j = 1, 2, \cdots, N)$ and $\omega_{N+1} = \omega + \Delta\omega_{N+1}$, where $\omega, \Delta\omega_0$, and $\Delta\omega_{N+1}$ are constants.

The inhomogeneity at both ends is related to the boundary conditions of the partial differential equation obtained by the continuum limit as shown in considering the synchronized solution of the type

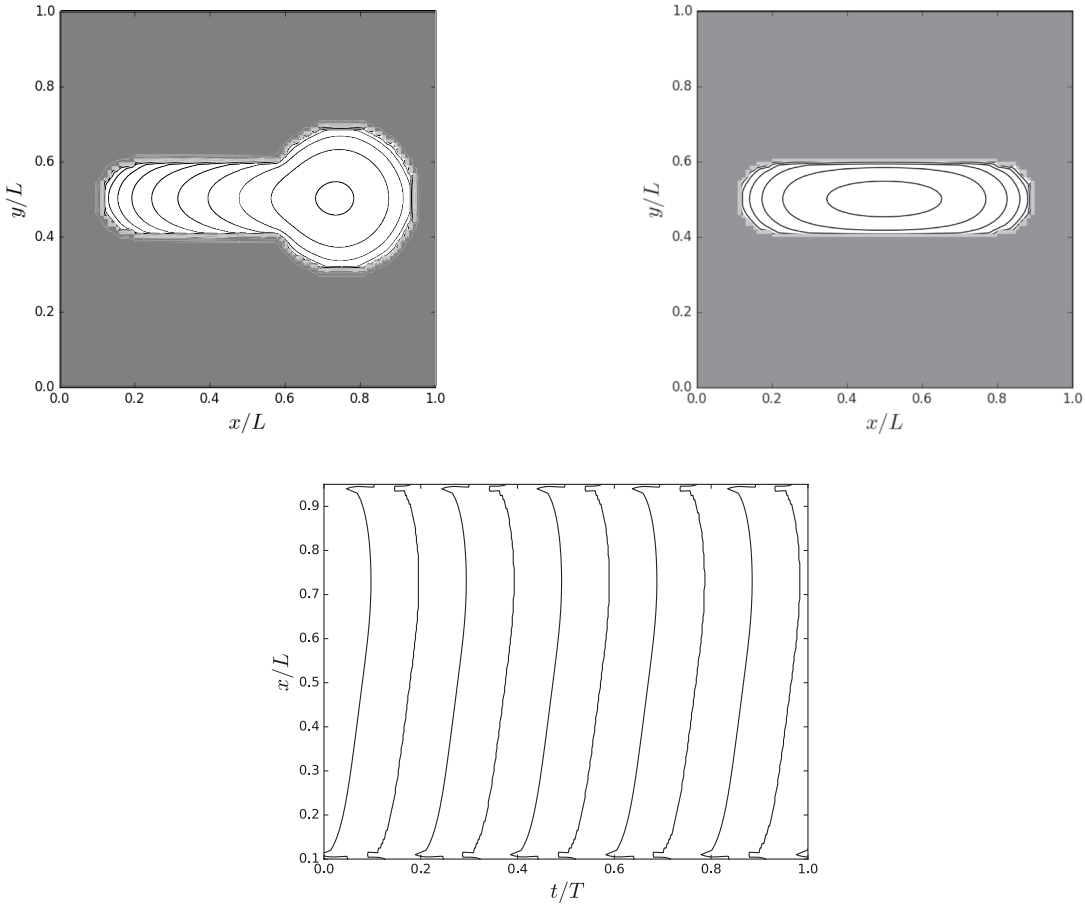

Figure 3. Top left: isophase lines at $\phi = n\pi/10$(n is an integer). The dark gray region and the light gray region are indicated by $\overline{B_i \cup B_b}$ and B_b, respectively. Top right: same as the left, but $r_2 = 0.1L$. Bottom: the spatiotemporal pattern of the isophase lines at $\phi = 2n\pi$ in the case of the tadpole shape along the line $y = L/2$. Isophase lines near the boundaries show sharp bends, but this is an artifact due to the contour algorithm of the software.

$$\phi_j = \Omega t + \alpha l j, \tag{7}$$

where Ω, the frequency of the synchronized state, and α, the increment of the phase per unit length (the phase gradient), are constants. It should be noted that equation (7) does not satisfy the whole set of equations (4)–(6), but approximately represents the behavior near each of the ends. To see this, we consider the case in which a synchronized state (7) that satisfies the set of equations (4) and (5), which represents the phases near the region where j is close to zero (locally synchronized state). Substituting the expression (7) into equations (4) and (5), we get

$$\Omega = \omega + \Delta\omega_0 + \tilde{k} f(-l\alpha) \tag{8}$$

$$\Omega = \omega + \tilde{k}\{f(l\alpha) + f(-l\alpha)\}. \tag{9}$$

These equations contain two unknowns, α and Ω. We easily obtain α by solving the equation $\Delta\omega_0 = \tilde{k} f(l\alpha)$, and Ω is obtained by equation (8) with the obtained value of α.

If the natural frequency is homogeneous at the end $j = 0$, i.e. $\Delta\omega_0 = 0$, and thus we obtain $(\alpha, \Omega) = (0, \omega)$; the phase of the synchronized state is also homogeneous. In the case $\Delta\omega_0 \neq 0$, $\alpha \neq 0$ in general. If $\Delta\omega_0/\tilde{k} \ll 1$, then α is obtained by using the approximation $f(x) \simeq f(0) + xf'(0) = xf'(0)$ ($f'(x) = \mathrm{d}f/\mathrm{d}x$) as

$$\alpha = \frac{\Delta\omega_0}{\tilde{k} l f'(0)}. \tag{10}$$

This formula shows that the phase increment between adjacent oscillators is proportional to the increment of the frequency at the end $\Delta\omega_0$. A similar formula is obtained at the other end, $j = N + 1$.

A continuum limit follows by regarding ϕ_j as the phase at the position $x = lj$, putting $L = l(N + 1)$, and replacing $k = \tilde{k} l^2$. Then, the gradient of the phase at $j = 0$, estimated by $(\phi_1 - \phi_0)/l$ is:

$$\frac{\phi_1 - \phi_0}{l} = \alpha = \frac{l\Delta\omega_0}{k f'(0)}. \tag{11}$$

In the limit $l \to 0$ with keeping L and $l\Delta\omega_0 = \beta^{(\mathrm{left})}$, we obtain

$$\frac{\partial\phi(0)}{\partial x} = \frac{\beta^{(\mathrm{left})}}{k f'(0)}. \tag{12}$$

Thus, the frequency difference at an end in the discrete system corresponds to the Neumann boundary condition with nonzero gradient in the continuum system.

Table 1. Values of a in synchronized states for both positive and negative values of b.

b	a	b	a
1	25.	−10	0.0604 697
0.1	3.598 07	−1	0.510 417
0.01	2.5856	−0.1	1.850 43
0.001	2.508 36	−0.01	2.418 85

We derive the continuum limit of equations (5) as:

$$\frac{\partial\phi}{\partial t} = \omega + \nu\frac{\partial^2\phi}{\partial x^2} + \mu(\frac{\partial\phi}{\partial x})^2, \tag{13}$$

$$\nu = -kf'(0), \quad \mu = kf''(0). \tag{14}$$

Here, we additionally assume $\nu > 0$, as $f'(0) < 0$, for stability [6]. If $f(x)$ has the particular form $f(x) = -\sin(x+\Theta) + \sin(\Theta)$, then $\nu = k\cos\Theta$ and $\mu = -k\sin\Theta$. The boundary conditions at both ends are:

$$\frac{\partial\phi(0)}{\partial x} = \frac{\beta^{(\mathrm{left})}}{kf'(0)}, \quad \frac{\partial\phi(L)}{\partial x} = -\frac{\beta^{(\mathrm{right})}}{kf'(0)}, \tag{15}$$

where $\beta^{(\mathrm{right})} = \lim_{l\to 0} l\Delta\omega_{N+1}$.

The effect of a non-zero gradient boundary can be clearly seen by considering a half-infinite system, such as $x \in [0, \infty)$, with the boundary condition

$$\frac{\partial\phi(0)}{\partial x} = \eta. \tag{16}$$

Because $f'(0) < 0$, negative η corresponds to positive $\Delta\omega_0$ in the discrete system. We assume the following solution

$$\phi(x,t) = \Omega t + \alpha x, \tag{17}$$

where Ω is the global synchronized frequency and α is a constant phase gradient. Because of the boundary condition,

$$\alpha = \eta \tag{18}$$

Substituting equation (17) in (13), we obtain

$$\Omega = \omega + \mu\alpha^2 = \omega + \mu\eta^2. \tag{19}$$

Therefore, the synchronized frequency Ω is determined by the boundary condition. Moreover, when $\eta < 0$, the solution given by equation (17) describes a phase wave sourced at the boundary $x = 0$. These properties are in accordance with those in the discrete system.

Thus, in order to explain the phase wave observed in slime molds, we considered a coupled oscillator system with the inhomogeneity in the peripheral part. We illustrated that a change in the frequency at the boundary in the discrete system corresponds to the Neumann boundary condition with a non-zero gradient in the phase diffusion equation.

4.2. Global synchronized solution and the effective peristaltic pumping for the tadpole-shaped slime mold

We consider the globally synchronized state of the coupled oscillator. To treat such a state, we consider the following one-dimensional phase diffusion equation:

$$\frac{\partial\phi}{\partial t} = \omega + \nu\frac{\partial^2\phi}{\partial x^2} + \mu(\frac{\partial\phi}{\partial x})^2, \tag{20}$$

where $\omega > 0, \nu > 0, \mu \neq 0$ are assumed. Also, the region assumed $-L \leqslant x \leqslant L$ with the boundary condition

$$\frac{\partial\phi(-L,t)}{\partial x} = \eta_-, \quad \frac{\partial\phi(L,t)}{\partial x} = \eta_+, \tag{21}$$

where η_+ and η_- are constants. Our purpose in this section is to show that a similar peristaltic pumping pattern as [10] is achieved by setting an appropriate boundary conditions, i.e. $\eta_\pm$ values. The solution of the equation (20) with the boundary conditions (21) is explicitly given in appendix.

According to [14], we estimate the characteristic values of the system parameters as follows. The value of ν is estimated by the diffusion coefficient of chemicals in the protoplasmic sol, $D = 4.4 \times 10^{-13}\,\mathrm{m\,s^{-1}}$. A typical length scale is estimated as $L = 150\ \mu$m, so that the length of the tail part of the tadpole-shape, $2L$, is 300 μm. A typical time scale is $T = 100$ s, the same order as the oscillation. Using these values, we nondimensionalize equation (20) by $t = T\tilde{t}, x = L\tilde{x}$ and obtain

$$\frac{\partial\phi}{\partial t} = 2\pi + \nu'\frac{\partial^2\phi}{\partial x^2} + \mu'(\frac{\partial\phi}{\partial x})^2, \tag{22}$$

where x and t are nondimensional values and the tildes are omitted, $\nu' = \frac{\nu T}{L^2}, \mu' = \frac{\mu T}{L^2}$. The estimated value gives $\nu' = 0.002$. We have no data to determine μ', but it is known that both ν and μ are proportional to D [6]. Considering this fact, our estimation of μ includes an order of unity to compare the mathematical results with the observations.

For the boundary condition $\eta_- = -5, \eta_+ = 0$ are adopted, but these values are just selected to represent the difference of the boundary gradients at the both ends, followed by $\eta_0 = -5$ and $\Delta\eta = 5$, which leads to the parameter P (definition is equation (A.5) in appendix) as $P = \frac{10}{Lb}$.

To relate figure 1 to the solution of a one-dimensional model (20) and (21), we assume that the synchronized state is given as $\phi(x,t) = g(x) + \omega_0 t$, where x and t means the coordinate representing a position along the body axis and time, respectively. Then the phase is constant along the line determined by $\phi(x,t) = \mathrm{const}$. We represent this line as $x = x(t)$ so that $x'(t) = \frac{\mathrm{d}x}{\mathrm{d}t} = -\frac{\omega_0}{g'(x)}$ ($g'(x) = \frac{\mathrm{d}g}{\mathrm{d}x}$). Figure 1 indicates that $x'(t) \geqslant 0$ and x' are relatively small when x is small, and large where x is large. In terms of $g'(x)$, $g'(x) \leqslant 0$ and $|g'|$ are relatively large where x is small, and is close to zero where x is large.

Using equation (20), we obtain the differential equation of $g(x)$ as

$$g''(x) = a - b(g'(x))^2,\ a = \frac{\omega_0 - 2\pi}{\nu'}, b = \frac{\mu'}{\nu'} = \frac{\mu}{\nu}. \tag{23}$$

Introducing $v(x) = g'(x)$, the equation of $v(x)$ is given as

$$v'(x) = a - b(v(x))^2 (|x| < L), v(\pm L) = \eta_\pm, \tag{24}$$

where $v'(x) = dv/dx$. We note that the synchronized frequency ω_0 is given by a obtained by solving equations (23) and (24): $\omega_0 = 2\pi + \nu' a$. Letting $\eta_+ = 0, \eta_- = -5$ and using the

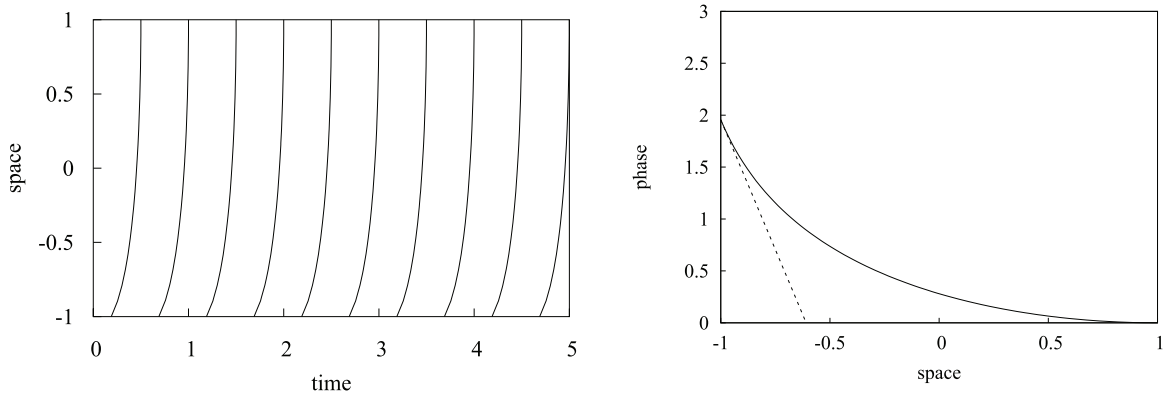

Figure 4. Left: contours of the constant phases ($\phi = n\pi +$ const.). Right: spatial distribution of the phase. The gradient of the line is η_-. ($b = -1$).

general formulae in appendix, we have the globally synchronized solutions, which do not describe a simple plane wave in which $g(x)$ is linear to x. The formulae depends on the sign of b, and typical values of a and b are listed in table 1.

In all cases listed, however, the synchronized frequency is almost the same as the natural frequency (the difference is less than 1%). Spatio-temporal diagram of the constant phase and $\phi(x)$ for $b = -1$ are shown in figure 4, which shows a qualitative agreement with figure 1, despite the very simple model. Although solutions with different values and signs of b satisfied the same boundary conditions, the transition region of the phase velocity is different. If $b < -1$, the region affected by the boundary condition at $x = -1$ becomes narrower. On the other hand, if $b > -1$, a larger region is affected by the boundary condition at $x = -1$.

As discussed in this section and illustrated in appendix, the phase gradient at the boundary modulates the phase wave propagation for a synchronized state in a region near the boundary. If the value of the phase gradient differs at both ends, we can regard the whole region as a set of regions so that the phase wave property in each region is mainly determined by the phase gradient at one end. The typical area (or length) of such region depends on the set of the values of the phase gradient at the ends. Our results suggest how the phase wave propagation in a two dimensional case was determined by the boundary condition in the tail region, where the boundary shape affects the area of influence.

5. Concluding remarks

In conclusion, we have considered the inhomogeneous wave propagation of the slime mold. Every organism has a boundary that divides the individual and the environment, so that the region near the boundary should be strongly affected by the environment. It is a natural assumption to suggest some kind of heterogeneity at the boundary. Based on this viewpoint, we considered heterogeneity of the boundary in discrete coupled oscillators as a model of contraction waves in slime molds. We have shown that the discrete model is reduced to the phase diffusion equation with nonzero flux boundary conditions under an appropriate continuum limit.

Our derived phase diffusion equation provides analytical inhomogeneous phase wave solutions, which is essential for the transport of chemicals in the tadpole shaped slime mold. Two models were considered to compare with the measured data of the phase distribution of a tadpole shape slime mold. One was a two-dimensional model that has a slightly higher natural frequency in the region of the boundary and the tadpole-like body shape being considered. The other was a one-dimensional model that has different gradients at both boundaries. Analytical solutions for both are obtained. In both models, we observed heterogeneous phase wave solutions and a slow phase wave in a small region at the end of the tail similar to the wave pattern in slime mold.

While many studies have suggested the existence of self-sustained biochemical oscillators in *Physarum* plasmodium, a primary oscillator is not known yet. One of the more likely possibilities is a Ca^{2+} oscillator [11], which may be derived by biochemical processes: (1) Ca^{2+}-induced Ca^{2+} release in transmembrane Ca^{2+} transport and/or (2) mechano-chemical interactions of actin with the other actin-related proteins and Ca^{2+}. As a result, Ca^{2+} can play a critical role in the rhythmicity of the contraction-relaxation cycle.

Biochemical kinetics of Ca^{2+} oscillations is already well-studied from a general point of view, and one of the most elementary and fundamental models is the 2-pool model, which has been well-examined [11]. In this model, the frequency of Ca^{2+} oscillations depends on the balance between inflow through a Ca^{2+} channel and outflow through a Ca^{2+} pump in the cell membrane. This implies that the ratio of surface area of membrane and volume at the intracellular vicinity of the cell membrane vary in a complex cellular shape owing to different curvatures of the membrane. This is a possible cause of inhomogeneous boundary conditions, if the densities of the Ca^{2+} pump and channels are distributed homogeneously on the membrane surface.

However, recent studies show that channel proteins often tend to form in large clusters; therefore, the inhomogeneity of the channel distribution is also a possible cause of inhomogeneous boundary conditions. We note that not only the oscillation mechanism alone, but also the body shape and the cytoskeletal network might contribute to the oscillation properties [16, 17]. As inhomogeneous boundary conditions

Table A1. Categories of solution ($b > 0$). P.D. stands for the 'propagation direction' of the phase wave. The abbreviations of 'one direction', 'pos. & neg', and 'no' stand for propagation in one direction, the coexistence of the waves propagating in positive and negative directions, and no propagation, respectively.

	Case	$v(x)$	P.D.	ω_0
(I)	$\Delta\eta > 0$	tanh-type	One direction/ pos. & neg.	$\omega_0 > \omega$
(II)	$\Delta\eta = 0$	Constant	One direction/no	$\omega_0 > \omega$
(III)	$\Delta\eta < 0, P < 0$	coth-type	One direction	$\omega_0 > \omega$
(IV)	$\Delta\eta < 0, P = 0$	$1/x$-type	One direction	$\omega_0 = \omega$
(V)	$\Delta\eta < 0, P > 0$	tan-type	One direction/ pos. & neg.	$\omega_0 < \omega$

Table A2. Categories of solution ($b < 0$).

	Case	$v(x)$	P.D.	ω_0
(V')	$\Delta\eta > 0, P > 0$	tan-type	One direction/ pos. & neg.	$\omega_0 > \omega$
(IV')	$\Delta\eta > 0, P = 0$	$1/x$-type	One direction	$\omega_0 = \omega$
(III')	$\Delta\eta > 0, P < 0$	coth-type	One direction	$\omega_0 < \omega$
(II')	$\Delta\eta = 0$	Constant	One direction/no	$\omega_0 < \omega$
(I)	$\Delta\eta < 0$	tanh-type	One direction/ pos. & neg.	$\omega_0 < \omega$

are possible in amoeboid movement, clarifying the effects of various boundary conditions is an important consideration requiring further study. Our study also suggests that it is essential to consider appropriate boundary conditions when modeling the behavior of organisms interacting with their surrounding environment.

Acknowledgments

Part of this work was supported by KAKENHI, 23540433, 26310202, and the Cooperative Research Program of 'Network Joint Research Center for Materials and Devices'.

Appendix. Analysis of the phase diffusion equation with Neumann boundary conditions

We consider the phase diffusion equation (20)

$$\frac{\partial\phi}{\partial t} = \omega + \nu\frac{\partial^2\phi}{\partial x^2} + \mu(\frac{\partial\phi}{\partial x})^2, \tag{A.1}$$

where $\omega > 0, \nu > 0, \mu \neq 0$ are assumed. The region is $[-L, L]$ and Neumann boundary conditions are defined by

$$\frac{\partial\phi(-L,t)}{\partial x} = \eta_-, \quad \frac{\partial\phi(L,t)}{\partial x} = \eta_+. \tag{A.2}$$

The synchronized solution of this equation of the type $\phi(x,t) = g(x) + \omega_0 t$ is considered, where the phase profile $g(x)$ and the synchronized freqeuncy ω_0 are to be determined. We note that as a frame of reference, the phase wave propagates in positive x-direction if $g'(x) < 0$ and vise versa. By

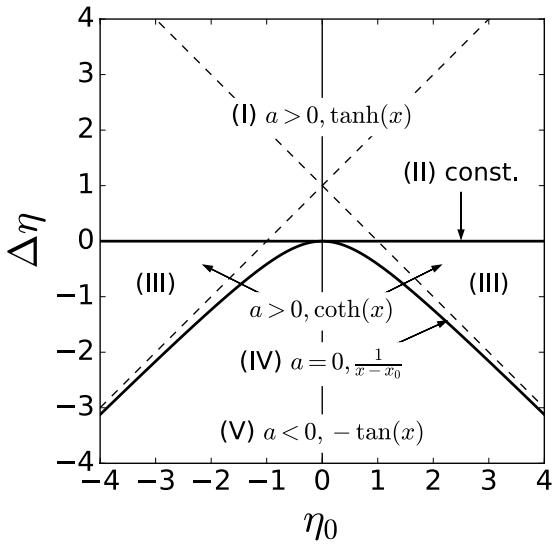

Figure A1. Diagram of the solution in the case $b > 0$. This diagram shows how (η_+, η) (equivalently, $(\eta_0, \Delta\eta)$) determines the sign a and the function of the solution.

substituting this solution into equation (A.1), and introducing $v(x) = g'(x)$, we obtain

$$v'(x) = a - b(v(x))^2, \quad v(\pm L) = \eta_\pm, \tag{A.3}$$

where

$$a = \frac{\omega_0 - \omega}{\nu}, b = \frac{\mu}{\nu}. \tag{A.4}$$

We note that the sign of $v(x)$ determines the propagation direction. The ordinary differential equation in (A.3) can be solved for given b and $\eta_\pm$. Below we show that different expressions for $v(x)$ and a are obtained depending on the set of b and $\eta_\pm$.

For convenience, we introduce

$$P = \eta_0^2 - (\Delta\eta^2 - \frac{2\Delta\eta}{Lb}), \ (\eta_0 = \eta_+ + \eta_-, \ \Delta\eta = \eta_+ - \eta_-), \tag{A.5}$$

which is used as well as $\Delta\eta$ for the classification of the solution. Below, we classify the solutions according the signs of $b, \Delta\eta$, and P.

Solutions for $b > 0$

(I) Case of $\Delta\eta > 0$. One can show that the solution exists for $a > 0$ as

$$v(x) = \sqrt{\frac{a}{b}}\tanh(\sqrt{ab}\,(x - x_0)), \tag{A.6}$$

with which the values of a and x_0 are further determined using equation (A.3). The direction of the phase wave changes at $x = x_0$ if $|x_0| < L$. The condition $a > 0$ implies $\omega_0 > \omega$.

(II) Case of $\Delta\eta = 0$.

$$v(x) = \eta, \quad a = b\eta^2 (\geqslant 0), \tag{A.7}$$

where $\eta = \eta_\pm$. When $a > 0$, $g(x)$ and the phase is monotonic, therefore, the phase wave propagates in one direction. Also $\omega_0 \geqslant \omega$ because $a \geqslant 0$.

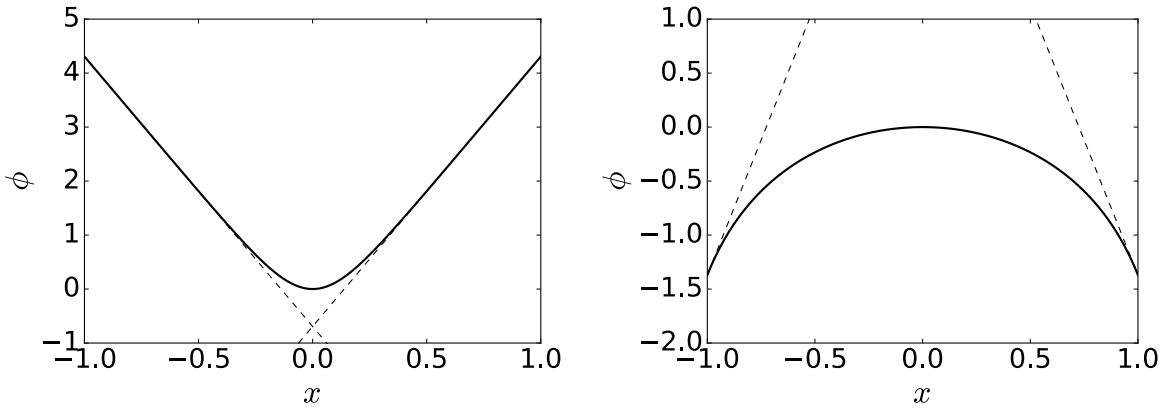

Figure A2. Phase distribution $\phi(x,0) = g(x)$ for the case $L = b = 1$. Left: $\eta_0 = 0, \Delta\eta = 10$ (tanh type). Right: $\eta_0 = 0, \Delta\eta = -10$ (tan type).

(III) Case of $\Delta\eta < 0$ and $P < 0$. One can show that the solution exists for $a > 0$ as

$$v(x) = \sqrt{\frac{a}{b}}\coth(\sqrt{ab}\,(x - x_0)). \tag{A.8}$$

Because the sign of v does not change in $[-L, L]$, $g(x)$ is monotonic and the phase wave propagates in one direction. Also, $\omega_0 > \omega$ because $a > 0$.

(IV) Case of $\Delta\eta < 0$ and $P = 0$. One can show that the solution exists for $a = 0$ as

$$v(x) = \frac{1}{b(x - x_0)}. \tag{A.9}$$

Because the sign of v does not change in $[-L, L]$, $g(x)$ is monotonic and the phase wave propagates in one direction. Also, $\omega_0 > \omega$ because $a > 0$.

(V) Case of $\Delta\eta < 0$ and $P > 0$. One can show that the solution exists for $a < 0$ as

$$v(x) = -\sqrt{-\frac{a}{b}}\tan(\sqrt{-ab}\,(x - x_0)). \tag{A.10}$$

Because the sign of v can chance in $[-L, L]$, $g(x)$ may have a peak in $[-L, L]$, thus, the direction of the phase wave may change at a certain point satisfying $v(x) = 0$ if the point is in the region $[-L, L]$. The condition $a < 0$ implies $\omega_0 < \omega$.

Solutions for $b < 0$

For $b < 0$, by introducing

$$\tilde{v} = -v, \quad \tilde{a} = -a, \quad \tilde{b} = -b,$$

we can rewrite equation (24) as

$$\tilde{v}'(x) = \tilde{a} - \tilde{b}(\tilde{v}(x))^2, \quad \tilde{v}(\pm L) = -\eta_{\pm}. \tag{A.11}$$

Because of $\tilde{b} = -b > 0$, the solutions of (A.11) are obtained as seen in section 5. For classification, we introduce

$$\tilde{P} = \tilde{\eta}_0^2 - (\Delta\tilde{\eta}^2 - \frac{2\Delta\tilde{\eta}}{L\tilde{b}}), \tag{A.12}$$

which is actually the same as P because $\Delta\tilde{\eta} = \tilde{v}(L) - \tilde{v}(-L) = -\Delta\eta, \tilde{\eta}_0 = \tilde{v}(L) + \tilde{v}(-L) = -\eta_0$.

Summary

The solution table is shown in tables A1 and A2. For the cases $b > 0$, the classification diagram is given in $(\eta_0, \Delta\eta)$-space (figure A1).

These solutions $v(x)$ connect both boundaries smoothly and monotonically but the function of the shape determines the shape details. For instance, the difference between the tanh type and tan type is shown in figure A2. Although all the obtained functions $v(x)$ connect the boundaries smoothly, the details of their shapes are different. For instance, as shown in figure A2, the phase distributions $\phi(x,0) = g(x)$ for the tanh-type (case (I)) and the tan-type (case (V)) are clearly different. Here, $b = 1$ is fixed and the boundary gradient has the same magnitude but with a different sign. We remark that the phase equation is not invariant under $\phi \to -\phi$ because of the term $(\partial\phi/\partial x)^2$, so this difference is expected. General Neumann boundary conditions can generate various phase waves, in addition to uniformly propagating phase waves. For example, as shown in figure A2 (left), the tanh type solution may have coexistent left- and right-propagation waves without any source of the wave inside the system region. Another solution of the tan type is displayed in figure A2(right), which is similar to figure A2(left) in a sense that both left- and right-propagation waves coexist. However, there is a distinct difference between the two wave types: in the tanh type solution, the phase velocity of the wave is almost uniform except near the region where counter-propagating waves collide, whereas in the tan type solution the phase velocity of the wave varies smoothly.

References

[1] Kogan B Y, Karplus W J and Karpoukhin M G 1994 The effect of boundary conditions and geometry of 2D excitable medeia on properties of wave propagation *Int. Workshop on Dynamism and Regulation in Non-linear Chemical Systems* pp 79–81

[2] Starobin J and Starmer C 1996 Boundary-layer analysis of waves propagating in an excitable medium: medium conditions for wave-front-bstacle separation *Phys. Rev.* E **54** 430–7

[3] Zykov V S, Mikhailov A S and Muller S C 1997 Controlling spiral waves in confined geometries by global feedback *Phys. Rev. Lett.* **78** 3398–401
[4] Haas G, Bär M, Kevrekidis I G, Rasmussen P B, Rotermund H H and Ertl G 1995 Observation of front bifurcations in controlled geometries: from one to two dimensions *Phys. Rev. Lett.* **75** 3560–3
[5] Hoeller O, Toettcher J E, Cai H, Sun Y, Huang C H, Freyre M, Zhao M, Devreotes P N and Weiner O D 2016 Gβ regulates coupling between actin oscillators for cell polarity and directional migration *PLoS Biol.* **14** 1–36
[6] Kuramoto Y 1984 *Chemical Oscillations, Waves, and Turbulence* (New York: Dover)
[7] Kamiya N 1959 Protoplasmic streaming *Protoplasmatologia* **8** 1–199
[8] Kamiya N and Allen R (ed) 1964 *Primitive Motile Systems in Cell Biology* (New York: Academic)
[9] Miyake Y, Tabata S, Murakami H, Yano M and Shimizu H 1996 Environment-dependent self-organization of positional information field in chemotaxis of Physarum plasmodium *J. Theor. Biol.* **178** 341–53
[10] Matsumoto K, Takagi S and Nakagaki T 2008 Locomotive mechanism of Physarum plasmodia based on spatiotemporal analysis of protoplasmic streaming *Biophys. J.* **94** 2492–504
[11] Keener J and Sneyd J 2009 *Mathematical Physiology I. Cellular Physiology* (Berlin: Springer) pp 273–303
[12] Agladze K, Ágota Tóth, Ichino T and Yoshikawa K 2000 Propagation of chemical waves at the boundary of excitable and inhibitory fields *J. Phys. Chem.* A **104** 6677–80
[13] Ryaben'kii V S, Tsynkov S V and Turchaninov V I 2001 Global discrete artificial boundary conditions for time-dependent wave propagation *J. Comput. Phys.* **174** 712–58
[14] Iima M and Nakagaki T 2012 Peristaltic transport and mixing of cytosol through the whole body of Physarum plasmodium *Math. Med. Biol.* **29** 263–81
[15] Cross M C and Hohenberg P C 1993 Pattern formation outside of equilibrium *Rev. Mod. Phys.* **65** 851–1112
[16] Arai A, Kyozuka K and Nakazawa T 1999 Cytoplasmic Ca^{2+} oscillation coordinates the formation of actin filaments in the sea urchin eggs activated with phorbol ester *Cell Motil. Cytoskeleton* **42** 27–35
[17] Mayne R, Adamatzky A and Jones J 2015 On the role of the plasmodial cytoskeleton in facilitating intelligent behavior in slime mold physarum polycephalum *Commun. Integrative Biol.* **8** 1–11